Electronic Supplementary Information (ESI)

Tricolor Reversible Luminescence Switching of a Mechano-/Vapochromic Mononuclear Cu(I) Complex

Zhen Mao,[‡a] Hai-Jian Li,[‡a] Xue He,[a] Sui-Jun Liu,[a] He-Rui Wen,[a] Li-Hua He,[a] Jing-Lin Chen*[a,b]

[a] *Jiangxi Provincial Key Laboratory of Functional Molecular Materials Chemistry, School of Chemistry and Chemical Engineering, Jiangxi University of Science and Technology, Ganzhou 341000, People's Republic of China*

[b] *State Key Laboratory of Structural Chemistry, Fujian Institute of Research on the Structure of Matter, Chinese Academy of Sciences, Fuzhou 350002, People's Republic of China*

EXPERIMENTAL SECTION

General Procedures and Materials. All reactions were carried out under a nitrogen atmosphere using solvents treated with an appropriate drying reagent. Commercially available reagents were directly used without further purification unless otherwise stated.

Crystal Structural Determination. Crystal data of compounds **1-c** and **1-g** were collected on a Bruker D8 QUEST and a Bruker D8 VENTURE diffractometer, respectively, with graphite-monochromated Mo Kα radiation (λ = 0.71073 Å). The structures were solved via the direct method and refined by full-matrix least-squares on F^2 using the *SHELXTL* and *Olex*2 software packages.[1-3] All non-hydrogen atoms were anisotropically refined, whereas hydrogen atoms were yielded theoretically and assigned isotropic thermal parameters. Crystallographic data and structure refinement details are summarized in Table S1, and selected bond lengths and bond angles are listed in Table S2.

Physical Measurements. ^{1}H and ^{31}P NMR spectra were recorded on a Bruker Avance III NMR spectrometer. Fourier-transform infrared (FT-IR) spectra were obtained on a Bruker Optics ALPHA FT-IR spectrometer using KBr pellets. Elemental analyses (C, H, N) were performed with a PerkinElmer model 240C elemental analyzer. Thermogravimetric analysis (TGA) was carried out on a PerkinElmer Pyris Diamond/Netzsch TG-209 instrument under a nitrogen atmosphere at a heating rate of 10°C min^{-1}. Powder X-ray diffraction (PXRD) analyses were made on a PANalytical B.V. Empyrean diffractometer equipped with a Cu target and a graphite monochromator. PXRD pattern simulations were performed using single-crystal structure data and the diffraction-crystal module of Mercury (Hg) 3.0, where is freely available *via* the Internet at http://www.iucr.org. Electronic absorption spectra in CH_2Cl_2 were measured on a Shimadzu UV-2550 spectrometer. Emission spectra in CH_2Cl_2 solution and the solid state were recorded on a Hitachi F-4600 fluorescence spectrometer. Solid-state luminescence quantum yields (Φ) were determined using an Edinburgh F900 fluorescence spectrometer equipped with a thermoelectrically cooled Hamamatsu R3809 photomultiplier tube and an integrating sphere.

Computational Methodology. Density functional theory (DFT) and time-dependent DFT (TDDFT) calculations were performed to investigate the photophysical properties of compound **1-c**. The initial structure was taken from its crystallographic coordinates. Geometry optimizations of the ground-state (S_0) in CH_2Cl_2 solution were carried out using the PBE0 hybrid functional[4], combined with the 6-31G(d) basis set[5] for H, C, N, and P atoms, and the SDD basis set[6] for the Cu atom. To

characterize the absorption properties, 80 singlet excited states were calculated via TDDFT[7,8]. Two initial structural models were constructed from the crystallographic data of **1-c**: one containing the dpaH-NH···$OClO_3^-$ hydrogen bond, and the other without this interaction. The geometries of the triplet excited states (T_1) in a rigid matrix (both with and without the hydrogen bond) were optimized using the same computational protocol as for the solution-phase S_0 state. For the hydrogen-bonded model, the lattice coordinates of the ClO_4^- anion were fixed, and the NH···O distance was constrained to 2.000 Å. In contrast, for the non-hydrogen-bonded model, the anion was also kept fixed, and the NH···O distance was constrained to 2.800 Å. Dispersion effects were incorporated using Grimme's D3 correction[9]. All calculations were performed with the ORCA software package[10-11]. Electronic density plots of the frontier molecular orbitals were generated using Multiwfn 3.8[12] and visualized with VMD[13].

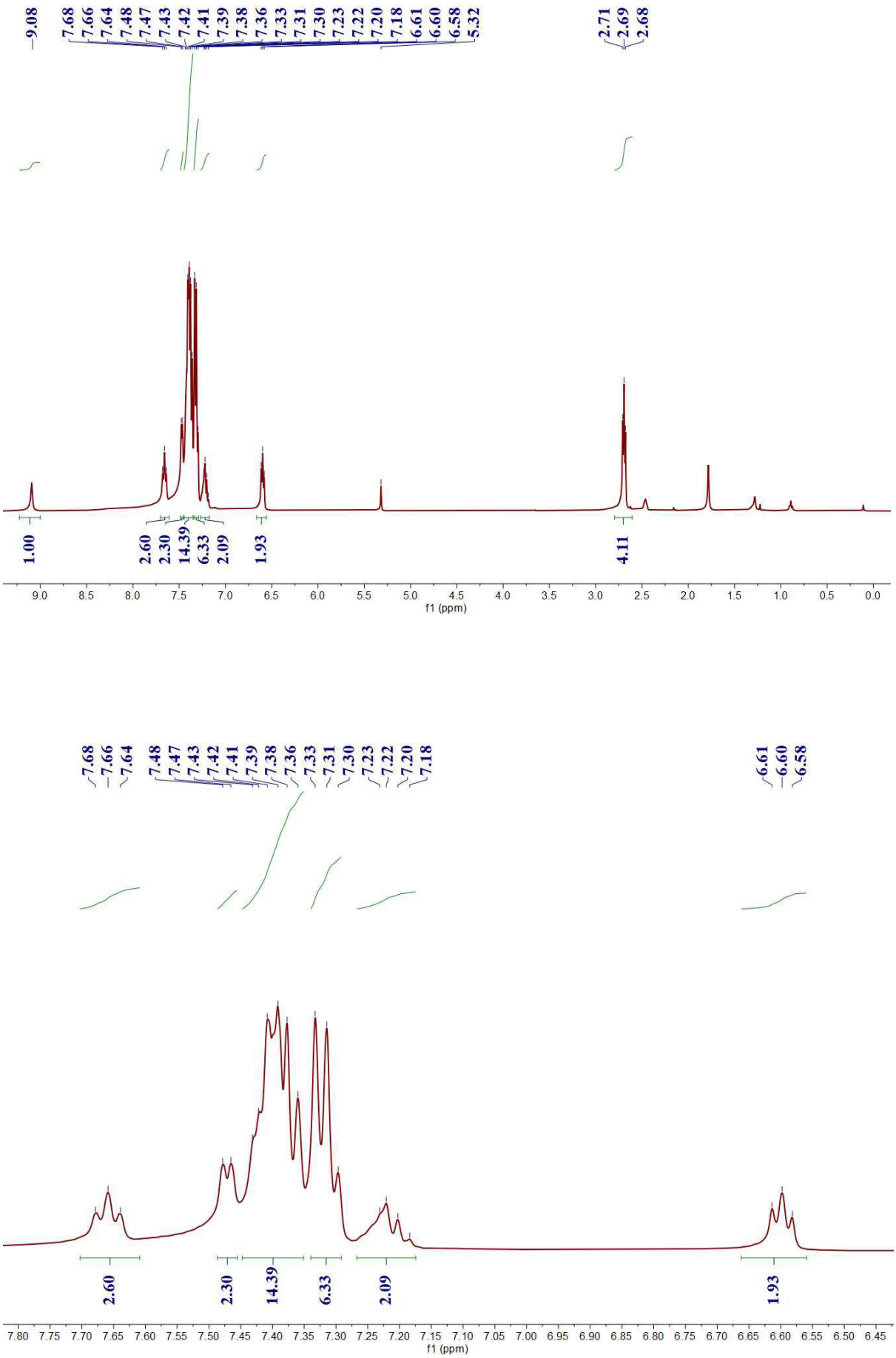

Fig. S1 ^{1}H NMR spectra of **1-c** in CD_2Cl_2.

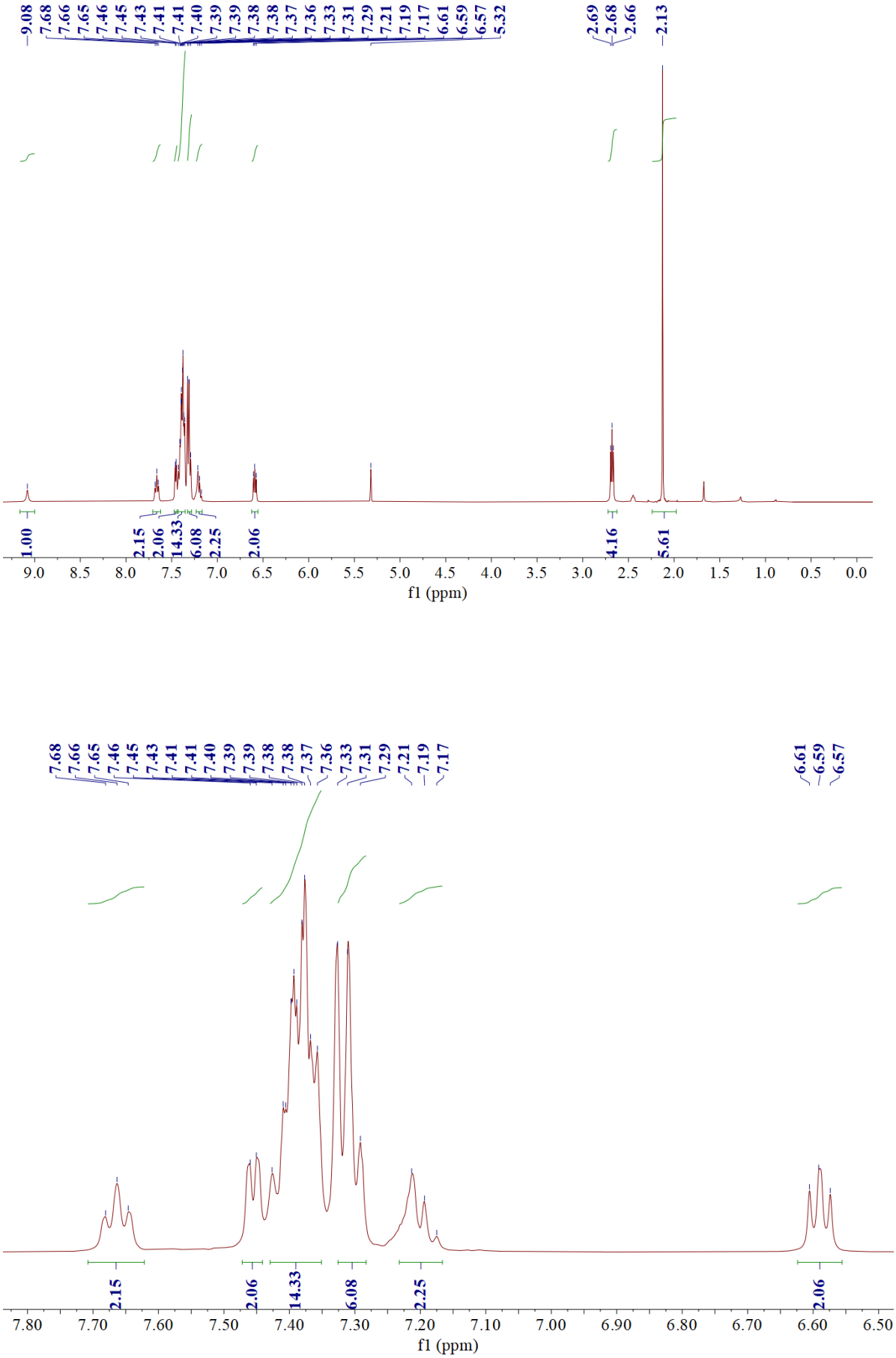

Fig. S2 ^{1}H NMR spectra of **1-g** in CD_2Cl_2.

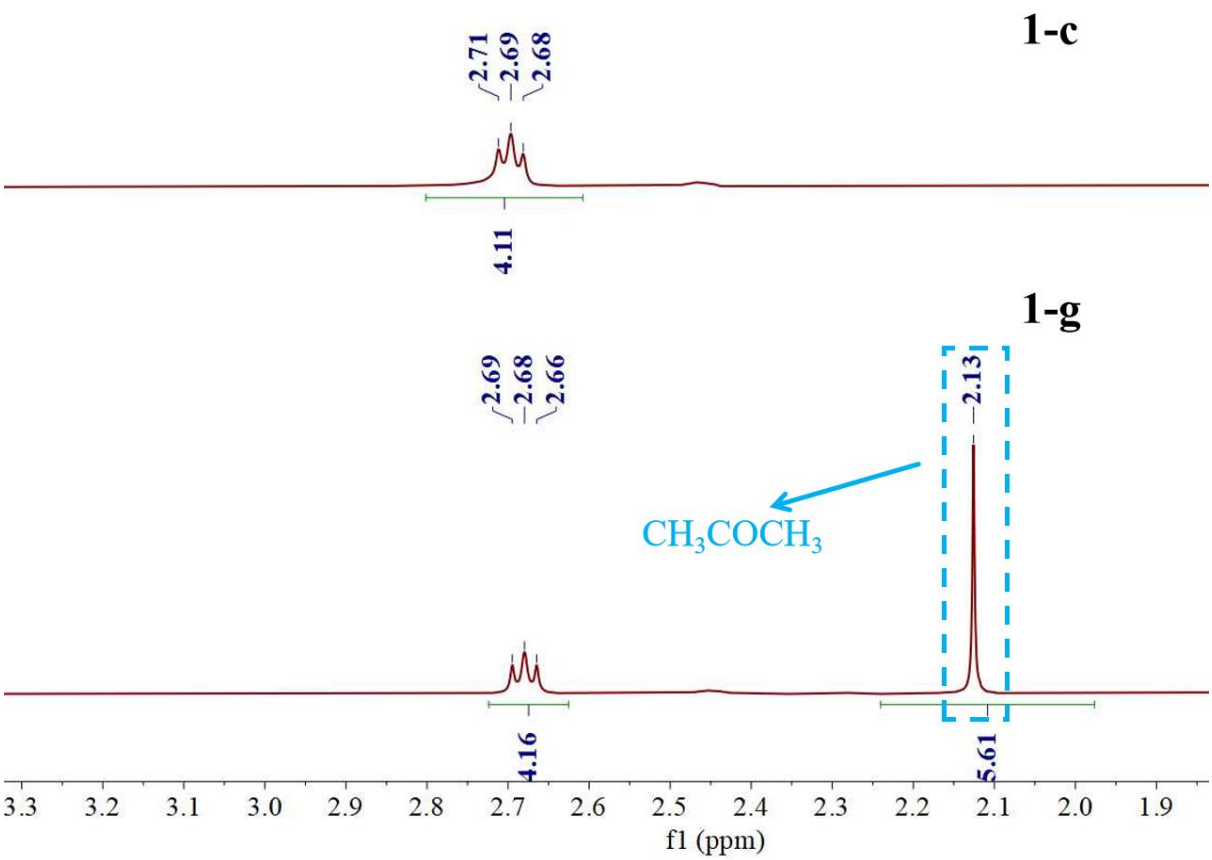

Fig. S3 ^{1}H NMR spectra of **1-c** and **1-g** in 1.9–3.3 ppm.

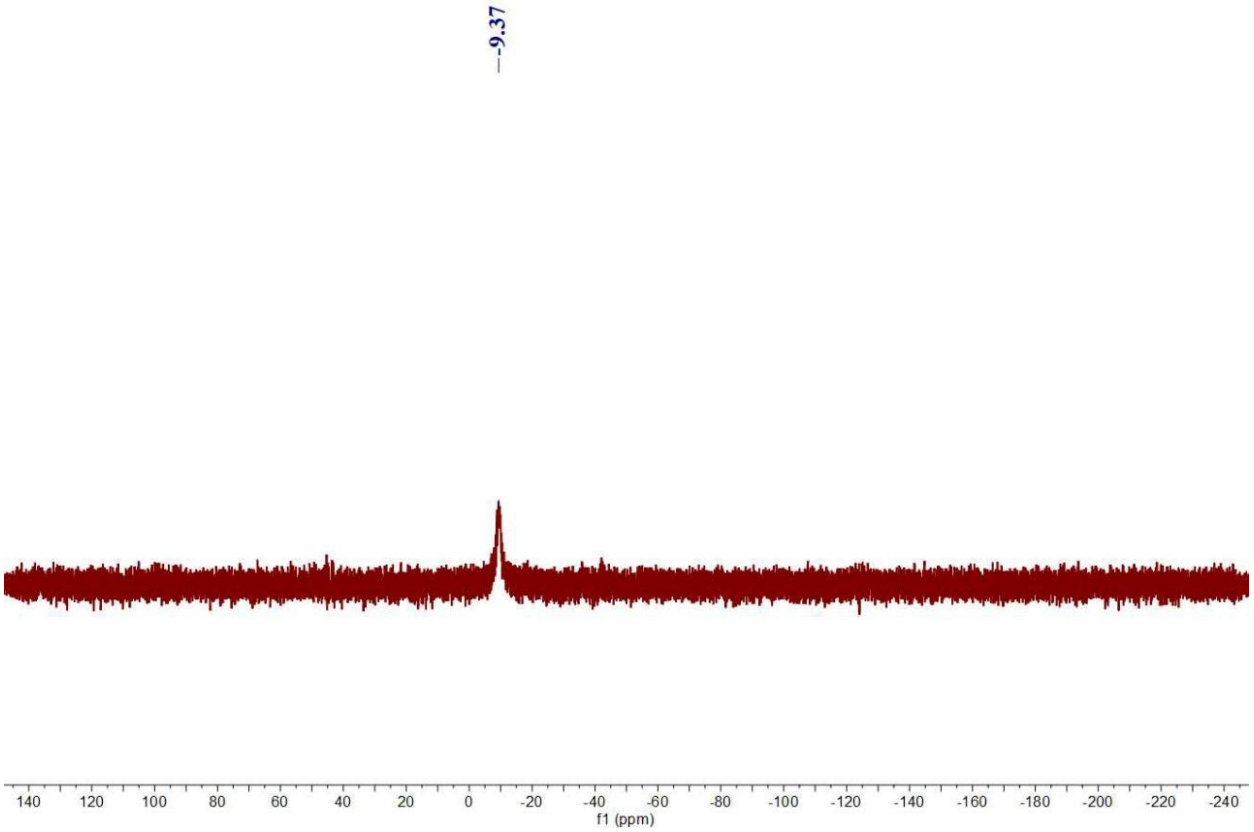

Fig. S4 ^{31}P NMR spectrum of **1-c** in CD_2Cl_2.

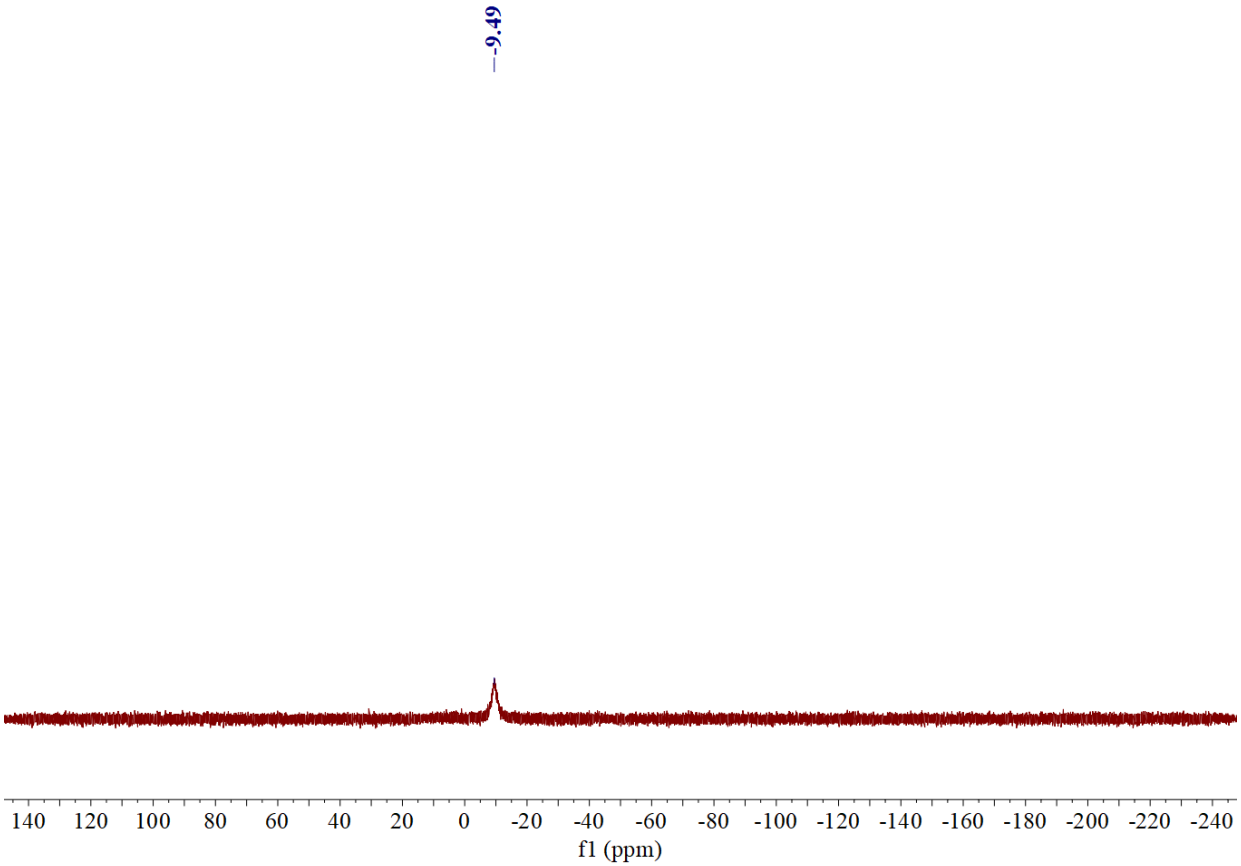

Fig. S5 ^{31}P NMR spectrum of **1-g** in CD_2Cl_2.

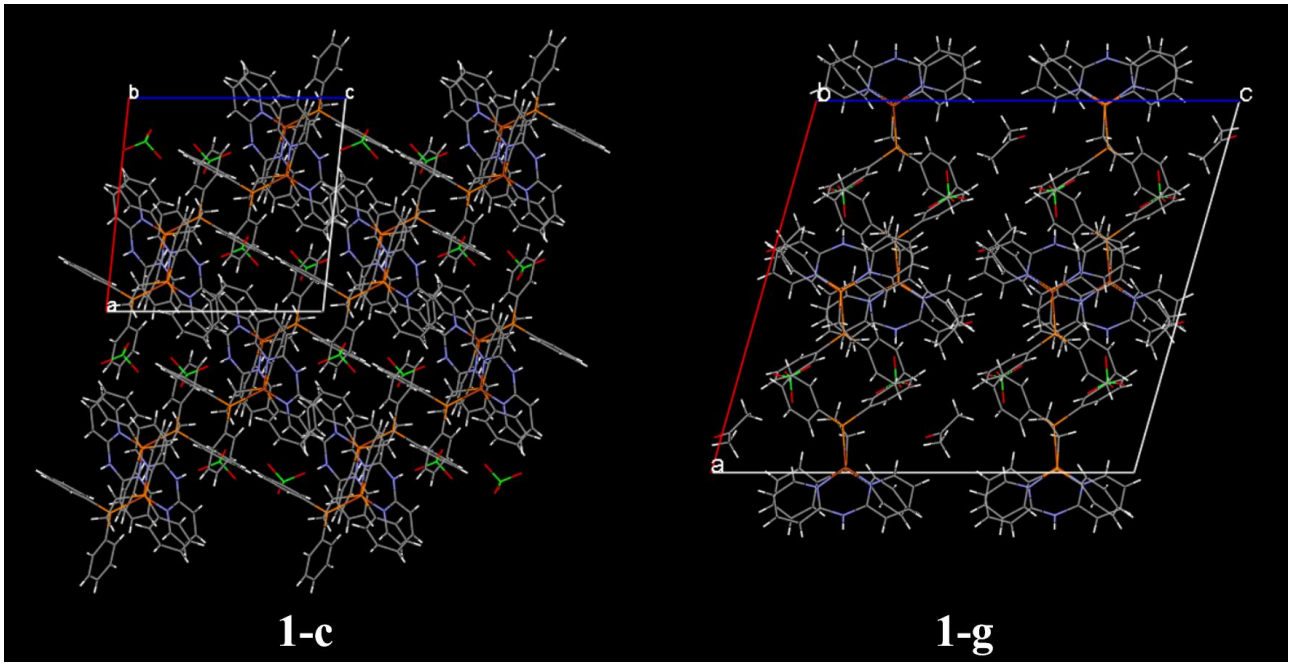

Fig. S6 Crystal packing diagrams of **1-c** and **1-g** viewed along the *b*-axis.

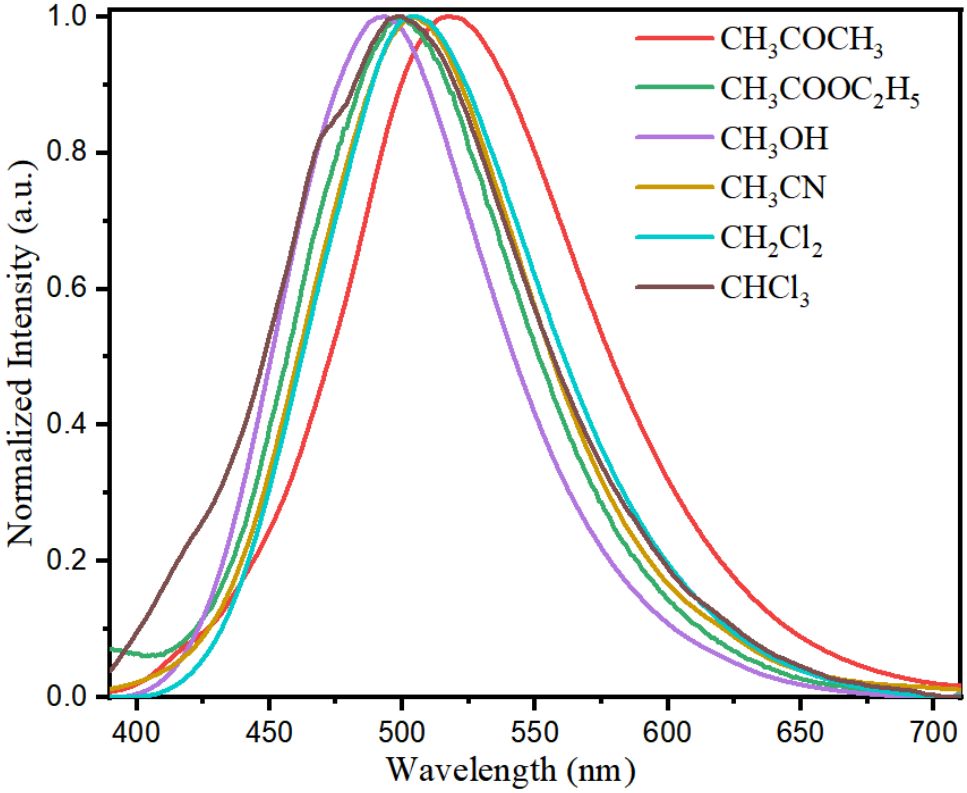

Fig. S7 Emission spectra of ground **1-g** after exposure to different organic vapors for more than 2.5 h.

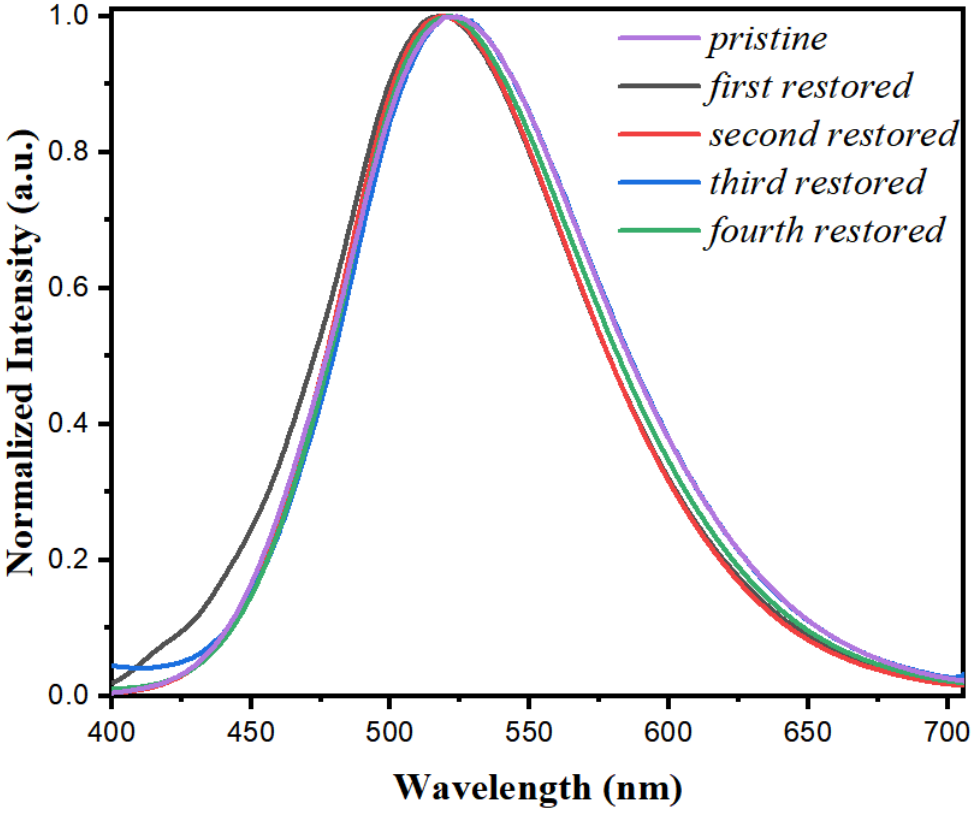

Fig. S8 Emission spectra of **1-g** upon grinding-acetone vapor fumigation cycles.

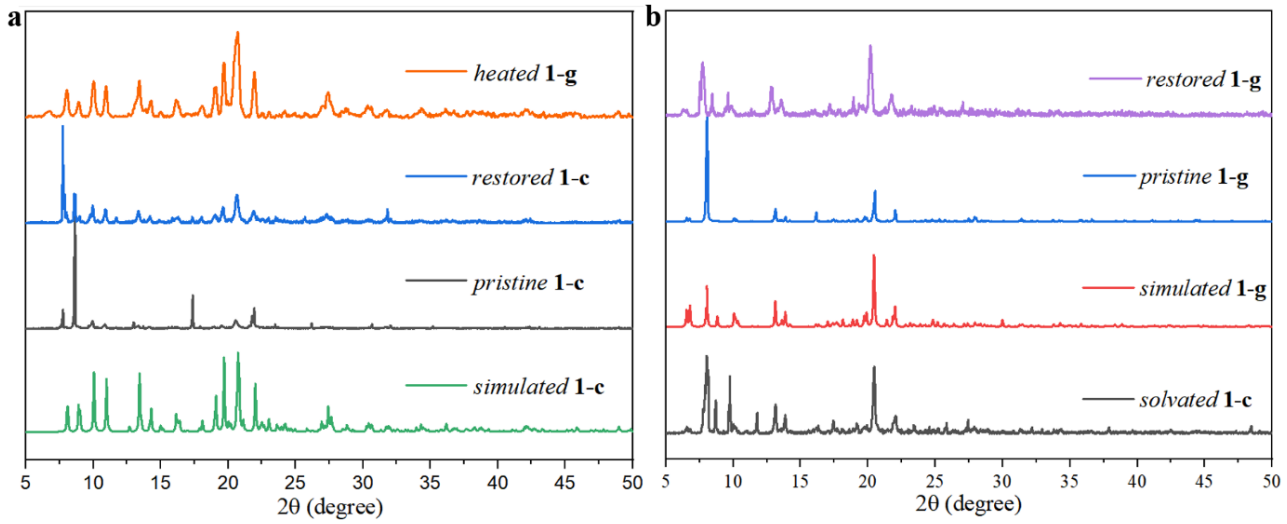

Fig. S9 Comparison of PXRD patterns for the corresponding phases of pristine **1-c** (a) and pristine **1-g** (b).

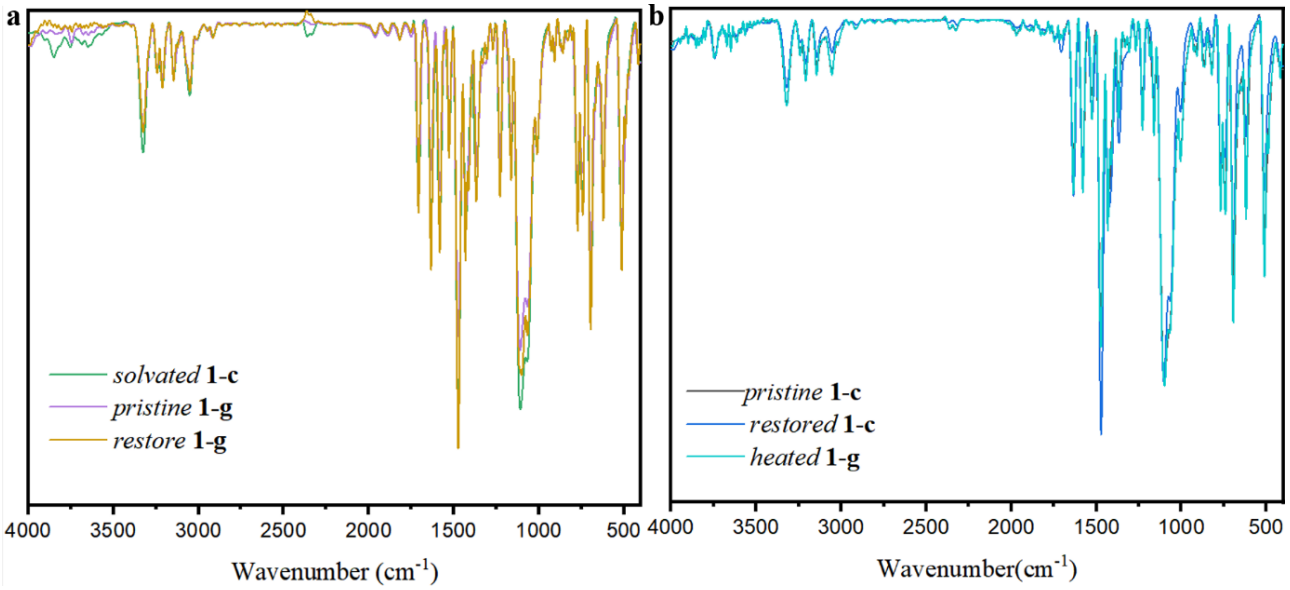

Fig. S10 Comparison of FT-IR spectra for the corresponding phases of pristine **1-g** (a) and pristine **1-c** (b).

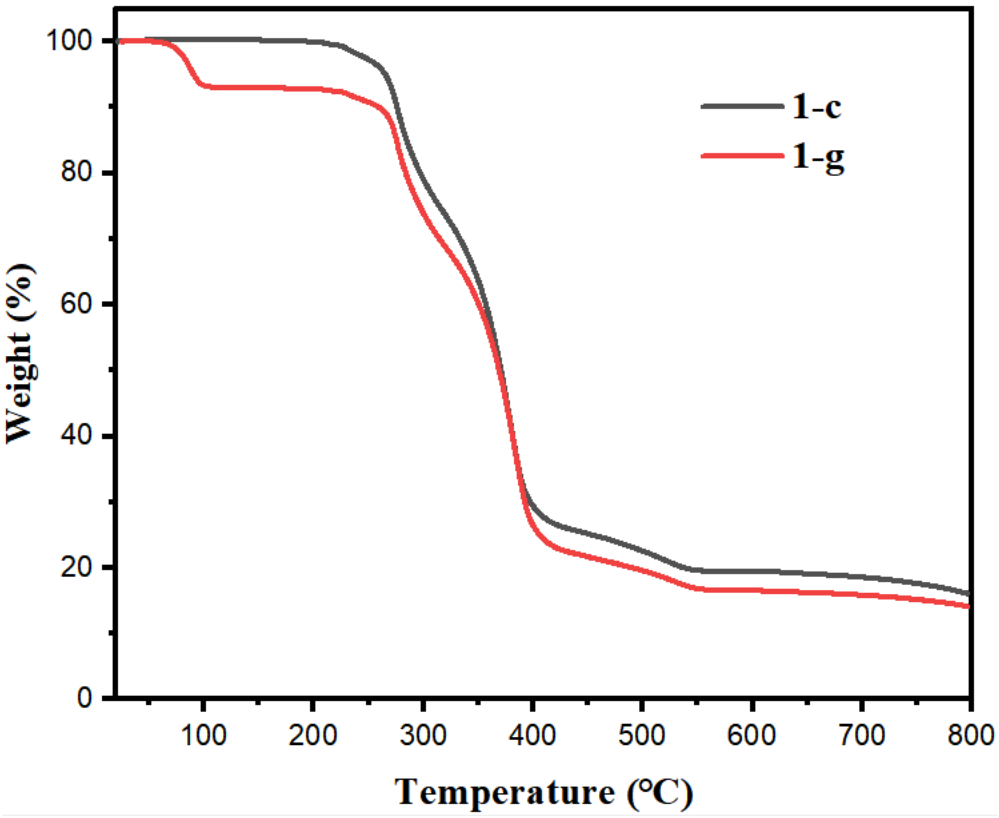

Fig. S11 TGA curves of pristine **1-c** and pristine **1-g**.

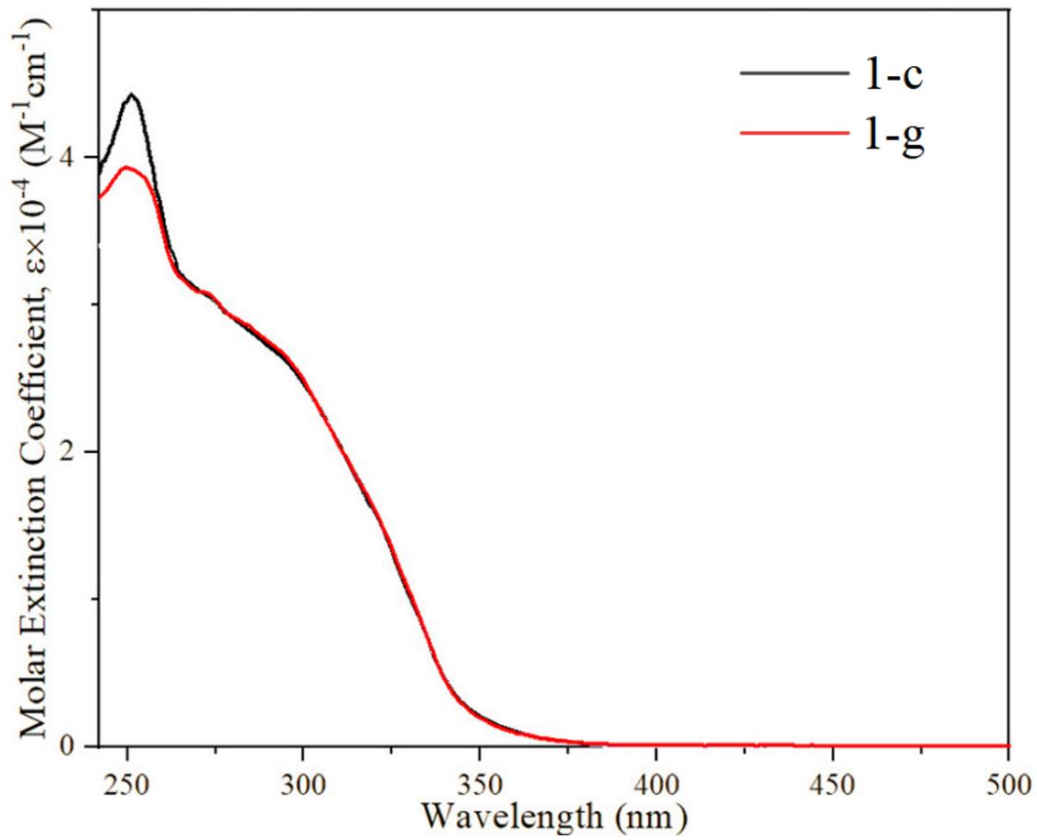

Fig. S12 UV-Vis absorption spectra of **1-c** and **1-g** in CH_2Cl_2 solution.

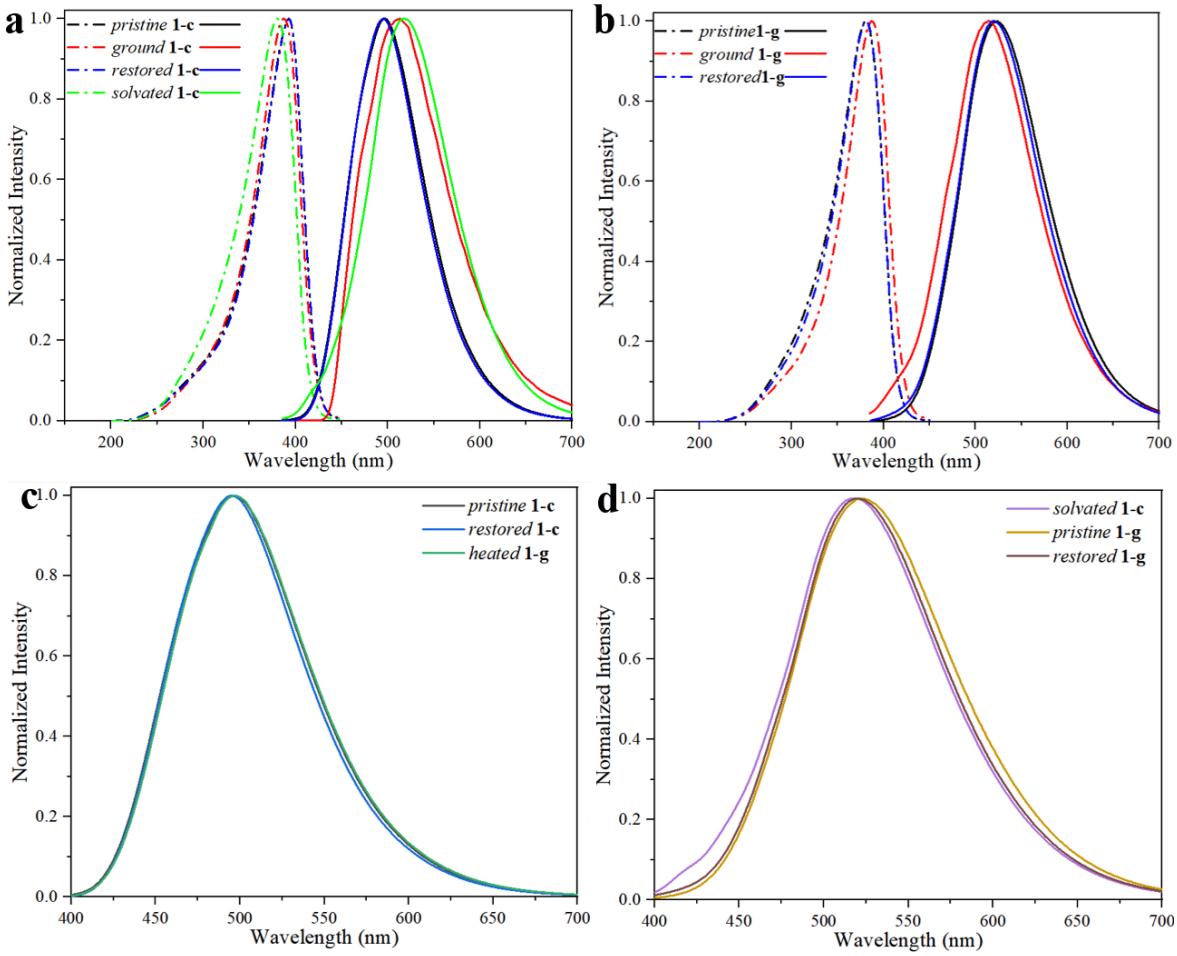

Fig. S13 Excitation (dash lines) and emission (solid lines) spectra of **1-c** (a) and **1-g** (b) in different states, and comparison of emission spectra for the corresponding phases of **1-c** (c) and **1-g** (d).

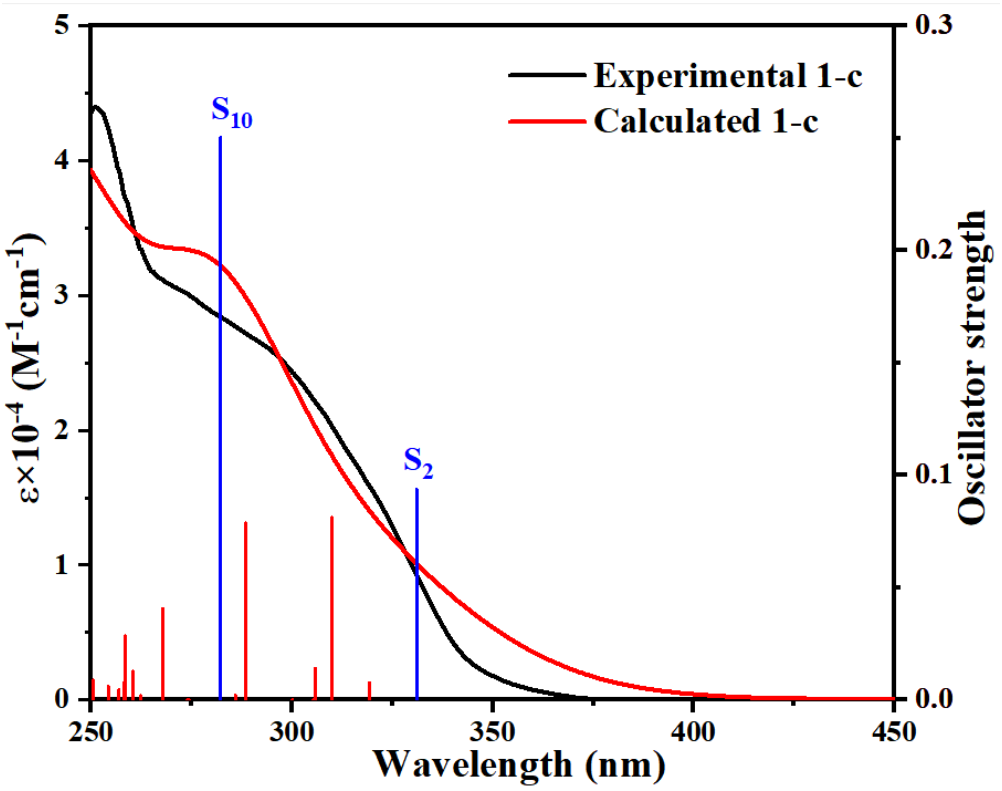

Fig. S14 Calculated (red vertical bars and red line) and experimantal absorption spectra (black line) of **1-c** in CH_2Cl_2.

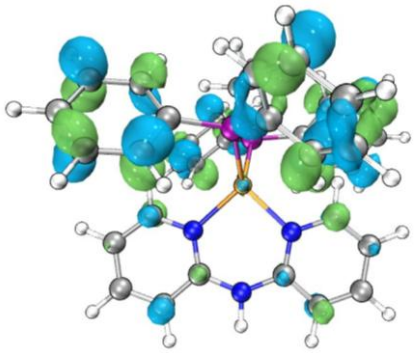	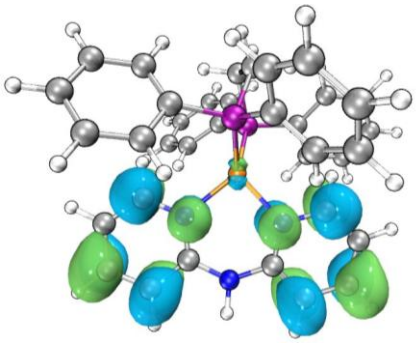	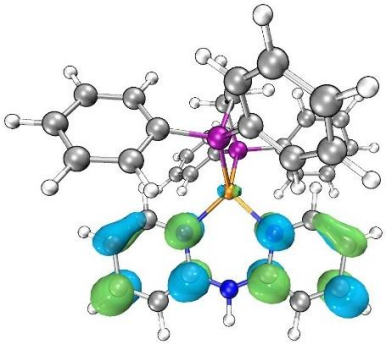
LUMO+7	LUMO+1	LUMO
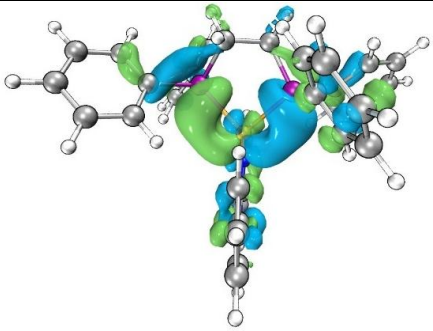	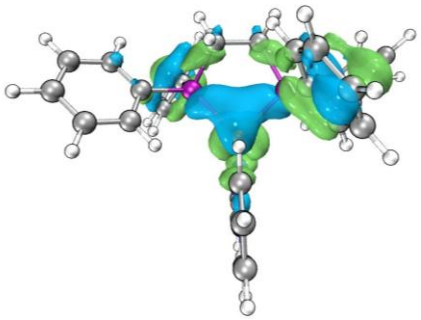	
HOMO	HOMO-1	

Fig. S15 Plots of frontier molecular orbitals involved in absorption transitions of **1-c** in CH_2Cl_2 media, calculated via TDDFT at the PBE1PBE level.

Table S1 Crystal Data and Structure Refinement Parameters of **1-c** and **1-g**

compound	**1-c**	**1-g**
formula	$C_{36}H_{33}ClCuN_3O_4P_2$	$C_{39}H_{39}ClCuN_3O_5P_2$
fw	732.58	790.66
T (K)	293(2)	270.5(3)
crystal system	monoclinic	monoclinic
space group	$P2_1/n$	$I2/a$
a (Å)	13.1077(8)	20.8314(18)
b (Å)	19.8491(13)	17.0911(16)
c (Å)	13.2457(9)	22.858(3)
α (deg)	90	90
β (deg)	96.073(2)	105.845(10)
γ (deg)	90	90
V (Å^3)	3426.9(4)	7828.9(14)
Z	4	8
ρ_{calc} (g cm^{-3})	1.420	1.342
μ (mm^{-1})	0.852	0.753
no. reflections collected	46942	40189
no. unique reflections	7858	8008
R_{int}	0.0525	0.1747
no. observed reflections	7858	8008
no. parameters	424	462
GOF on F^2	1.042	0.992
R_1 [$I > 2\sigma(I)$]	0.0543	0.0769
wR_2	0.1327	0.1946

Table S2 Selected Bond Lengths (Å) and Angles (deg) of **1-c** and **1-g**

compound	**1-c**	**1-g**
Cu1−N1	2.028(3)	2.015(5)
Cu1−N2	2.039(3)	1.995(5)
Cu1−P1	2.2787(11)	2.2666(19)
Cu1−P2	2.2860(10)	2.2387(18)
N1−Cu1−N2	92.78(13)	94.2(2)
N1−Cu1−P1	122.81(10)	109.36(17)
N1−Cu1−P2	116.49(10)	119.20(16)
N2−Cu1−P1	115.83(10)	121.73(17)
N2−Cu1−P2	121.04(9)	121.77(16)
P1−Cu1−P2	90.66(4)	92.14(7)

Table S3 Photoluminescence Data of **1-c** and **1-g** in Different States

compound	state	λ_{em} [nm]	Φ_{em} [%]
1-c	pristine	497	41
	ground	513	5
	restored	496	23
	solvated	520	17
1-g	pristine	522	22
	ground	513	3
	restored	520	17
	heated	497	11

Table S4. Absorption Transition Data of **1** in CH_2Cl_2 Media Calculated via TDDFT at the PBE1PBE Level

Es[a]	E (eV)/(nm)	Os[b]	Configuration	Assignment
S_2	3.75 eV/331 nm	0.0938	HOMO→LUMO+1 (97.2%)	^{1}MLCT/^{1}LLCT
S_{10}	4.39 eV/282 nm	0.2504	HOMO-1→LUMO (48.8%) HOMO→LUMO+7 (29.4%)	^{1}MLCT/^{1}LLCT

Table S5. Partial Molecular Orbital Compositions (%) of **1** in Optimized S_0 State (CH_2Cl_2 Media), calculated via TDDFT at the PBE1PBE Level

Orbital	Bond type	MO contribution (%)		
		Cu	dppe	dpaH
LUMO+7	π*(dppe)	15.22	71.96	12.82
LUMO+1	π*(dpaH)	3.46	7.14	89.40
LUMO	π*(dpaH)	1.24	1.42	97.34
HOMO	d(Cu)+π(dppe)	32.11	57.29	10.60
HOMO-1	d(Cu)+π(dppe)	45.54	45.25	9.21

Table S6. Partial Molecular Orbital Compositions (%) and Calculated Lowest-Lying Triplet Emission Energies of **1-c** (with NH···$OClO_3^-$ Hydrogen Bond) Calculated via TDDFT at the PBE0 Level

Orbital	Energy	λ_{em}^{Calc}	MO contribution (%)		
	(eV)	nm (eV)	Cu	dppe	dpaH
LUMO	-1.54	487 (2.54)	1.69	9.21	89.10
HOMO	-5.42		34.81	51.91	13.28

Table S7. Partial Molecular Orbital Compositions (%) and Calculated Lowest-Lying Triplet Emission Energies of **1-c** (without NH···$OClO_3^-$ Hydrogen Bond) Calculated via TDDFT at the PBE0 Level

Orbital	Energy	λ_{em}^{Calc}	MO contribution (%)		
	(eV)	nm (eV)	Cu	dppe	dpaH
LUMO	-2.39	520 (2.38)	3.81	10.16	86.03
HOMO	-5.65		29.78	60.90	9.32

REFERENCES

(1) G. Sheldrick, *Acta Cryst. Sect. A*, 2008, **64**, 112-122.

(2) G. Sheldrick, *Acta Cryst. Sect. A*, 2014, **70**, 1437.

(3) H. Puschmann, L. J. Bourhis, O. V. Dolomanov, R. J. Gildea, J. A. K. Howard, *Acta Cryst. Sect. A*, 2011, **67**, 593.

(4) J.P. Perdew, K. Burke, M. Ernzerhof, *Phys. Rev. Lett.*, 1996, **77**, 3865-3868.

(5) M.M. Francl, W.J. Pietro, W.J. Hehre, J.S. Binkley, M.S. Gordon, D.J. DeFrees and J.A. Pople, *J. Chem. Phys.*, 1982, **77**, 3654-3665.

(6) P.J. Hay, W.R. Wadt, *J. Chem. Phys*., 1985, **82**, 299-310.

(7) M.E. Casida, C. Jamorski, K.C. Casida, D.R. Salahub, *J. Chem. Phys*., 1998, **108**, 4439-4449.

(8) R.E. Stratmann, G.E. Scuseria, M.J. Frisch, *J. Chem Phys*., 1998, **109**, 8218-8224.

(9) S. Grimme, J. Antony, S. Ehrlich, H. Krieg, *J. Chem. Phys.*, 2010, **132**.

(10) F. Neese, *WIREs Comput. Mol. Sci.*, 2018, **8**.

(11) J. P. Perdew, K. Burke, and M. Ernzerhof, *Rev. Lett*. 1996, **77**, 3865.

(12) T. Lu, F. Chen, *J. Comp. Chem*., 2012, **33**, 580-592.

(13) W. Humphrey, A. Dalke, K. Schulten, *J. Mol. Graph*., 1996, **14**, 33-38.